# Structure and Dynamics of Cold-Adapted Enzymes as Investigated by Phosphorescence Spectroscopy and Molecular Dynamics Studies. 2. The Case of an Esterase from *Pseudoalteromonas haloplanktis*

**Sabato D'Auria,*,† Vincenzo Aurilia,† Anna Marabotti,‡ Margherita Gonnelli,§ and Giovanni Strambini§**

*Laboratory for Molecular Sensing, Institute of Protein Biochemistry, CNR, Naples, Italy, Laboratory of Bioinformatics, Institute of Food Sciences, CNR, Avellino, Italy, and Institute of Biophysics, CNR, Pisa, Italy*

*Received: May 9, 2009; Revised Manuscript Received: August 13, 2009*

Enzymes from psychrophiles display high catalytic efficiency at low temperatures. As a consequence, there is a lot of academic and industrial interest in investigating the molecular strategies adopted from these enzymes to work in conditions where other enzymes are almost inactive. Recently, a novel esterase activity was identified and isolated from the cold-adapted organism *Pseudoalteromonas haloplanktis*. The enzyme, named PhEST, is a dimer with a molecular mass of 60 kDa composed of two identical subunits. PhEST possesses four tryptophan residues that are homogenously dispersed in the protein tertiary organization. In this work, we used phosphorescence spectroscopy and molecular dynamics experiments to investigate the structural properties of PhEST. The obtained model structure of PhEST indicates that the environments of tryptophan residues W14 and W50 are characterized by limited conformational freedom. On the contrary, the environments of the tryptophan residues W181 and W197 are relatively mobile owing to enhanced fluctuations of residues 93−99 and 192−195, respectively, flexible loops that join segments of the protein secondary structure. The high-resolution phosphorescence spectrum in low-temperature glasses distinguishes two classes of Trp environments in PhEST structure: one class that is typical of compact internal hydrophobic sites, and the other class that is characteristic of disordered and/or partly solvent exposed regions. The phosphorescence lifetime of PhEST registered in fluid solution is invariably short, indicating that some Trp residues are in rather flexible superficial sites of the globular fold, whereas internal chromophores are strongly quenched by the proximity to Cys residues. Acrylamide and $O_2$ quenching studies pointed out that the internal protein site is compact and rigid, typical of $\beta$-barrel core structures. Every spectroscopic feature described in this work is well accounted for by the proposed model structure of PhEST.

## Introduction

Life has evolved the capacity to develop in a broad range of different environments. Extreme temperature adaptation represents a well-known example of how microbes have developed singular molecular strategies to live and thrive. This is illustrated for hot environments by thermophilic organisms, which are capable of living at temperatures near or above the boiling point of water. At the opposite thermal extreme, psychrophilic (cold-adapted) organisms are defined as those organisms having an optimal temperature for growth at about 15 °C or lower.[1] Some organisms have been described that are capable of metabolizing in snow and ice at −20 °C, and numerous psychrophile isolates have been characterized by their ability to proliferate at ≤0 °C and are restricted to <30 °C.[2]

Cold-adapted organisms have developed several strategies to compensate for the very slow metabolic rates that would occur at low temperatures. The majority of the enzymes isolated from cold-adapted organisms are characterized by a shift in the apparent optimum temperature of activity toward low temperature values with a concomitant decrease in their structural stability. Moreover, these enzymes generally exhibit a high reaction rate by decreasing the activation free energy barrier between the ground state and the transition state. This decrease is structurally accomplished by a reduction in the number of enthalpy-related interactions that need to be broken during the formation of the transition state.[2] Therefore, cold-adapted enzymes tend to exhibit flexible folds characterized by a relatively large specific activity at low temperatures. These apparently mutually exclusive properties indicate that an activity−stability trade-off exists in cold-adapted enzymes. Since amino acids involved in catalysis are generally conserved between cold and thermostable homologous biomolecules, the causes of flexibility must reside in other parts of the structure of the enzyme.[3,4] In fact, flexibility can be achieved by a combination of structural features such as a reduction in core hydrophobicity, decreased ionic and electrostatic interactions, increased charge of surface residues that promote increased solvent interaction, additional surface loops, substitution of proline residues by glycines in surface loops, a decreased arginine/lysine ratio, fewer interdomain and subunit interactions, and fewer aromatic interactions.[5]

Due to their interesting properties (a high specific activity and a low thermal stability), enzymes from cold-adapted organisms represent an interesting target for both fundamental research and biotechnological applications. Moreover, since it has been demonstrated that each psychrophilic enzyme adopts

* Corresponding author. Dr. Sabato D'Auria; Laboratory for Molecular Sensing; IBP-CNR Via Pietro Castellino, 111; 80131 Naples, Italy; Phone: +39-0816132250; Fax: +39-0816132277; Email: s.dauria@ibp.cnr.it.

† Institute of Protein Biochemistry.

‡ Institute of Food Sciences.

§ Institute of Biophysics.

10.1021/jp9043286 CCC: $40.75 
Published on Web 09/15/2009

its own adaptive strategy and that there is a continuum in the strategy of protein adaptation to temperature,[6] it is interesting to investigate the stability−flexibility−activity relationships for enzymes potentially useful in biotechnology.

In a recent work,[7] we have described the gene cloning, the expression and the purification of a recombinant protein with an esterase activity isolated from the antarctic organism *Pseudoalteromonas haloplanktis* TAC125 (PhEST).[8] PhEST is capable of growing in the presence of 15% NaCl and at temperatures ranging from 4 to 15 °C.[8] This enzyme, classified as a feruloyl esterase belonging to family 1 of carbohydrate esterase enzymes, shows a molecular mass of 60 kDa and exhibits an optimum activity at about 30 °C.[7,9]

A three-dimensional model of the protein structure was also realized, and the amino acid residues responsible for the catalytic activity of the protein were identified. Furthermore, the effect of temperature on the stability and flexibility of this cold-adapted enzyme was probed by Fourier-transform infrared spectroscopy and molecular dynamics (MD) studies.[10]

The aim of the present work is to investigate structural and dynamical features of PhEST by means of the protein intrinsic tryptophan phosphorescence spectroscopy. We found that the protein displays a rather unusual phosphorescence emission that is largely dominated by intramolecular quenching interactions. This feature is well accounted for by the predicted protein structural fold. An excellent agreement between spectroscopic and bioinformatics results permitted us to investigate the structural dynamics of PhEST at different temperatures.

## Materials and Methods

**Reagents.** All chemicals were of the highest purity grade available from commercial sources and, unless otherwise specified, were used without further purification. Acrylamide (99.9% electrophoretic purity) was from Bio-Rad Laboratories (Richmond, CA). Tris(hydroxymethyl)-aminomethane (Tris), spectral-grade glycerol, and NaCl Suprapur were from Merck (Darmstadt, Germany). Water, doubly distilled over quartz, was purified by using a Milli-Q Plus system (Millipore corp., Bedford, MA). All glassware used for sample preparation was conditioned in advance by standing for 24 h in 10% HCl Suprapur (Merck, Darmstadt).

**Bacterial Strains, Plasmids and Growth Condition.** *Pseudoalteromonas haloplanktis* TAC125[8] was grown to saturation at 4 °C in TYP broth (16 $g \cdot L^{-1}$ yeast extract, 16 $g \cdot L^{-1}$ bacto-tryptone, 10 $g \cdot L^{-1}$ sea salts at pH 7.5). The *E. coli* strains used in this study were TOP10F' (Invitrogen) and BL21(DE3) purchased from Novagen. The plasmids used for cloning the esterase were pGEM-T (Promega-USA) and pET28a (Novagen). Recombinant *E. coli* strains were cultured at 37 °C in Luria−Bertani broth supplemented with ampicillin or kanamycin.

**Isolation of the Esterase Gene from *Pseudoalteromonas haloplanktis* TAC125.** Genomic DNA from *P. haloplanktis* was extracted from bacterial cells using the commercial kit Wizard Genomic DNA prep supplied from Promega (USA). The gene encoding an esterase (PSHAa 1385) was amplified via PCR using two primers that define the N-terminal and C-terminal regions of the gene. The 5′ primer used in the amplification contained the ATG start codon and a *BamH1* site (bold-faced letters and underlined in the sequence, respectively): PA1385FW: TAGGATCCGGC**ATG**TTAGAAAATATCTCAAGTG. The 3′ primer PA1385RV1 had the following sequence 5′-AGGCTCGAGAAATCCT**AAT**AGTTATGCAGAC-3′ and was designed to insert a recognition site for the *XhoI* endonuclease (underlined) immediately upstream of the termination codon (bold-faced letters). The reaction was performed in a Mastercycle apparatus using as enzyme the *Taq* polymerase High Fidelity (La Roche, Germany) under the following conditions: denaturation at 95 °C for 5 min, followed by 30 cycles of denaturation at 95 °C for 1 min, annealing at 55 °C for 1 min, and extension at 72 °C for 1 min. The resulting DNA fragment was ligated into the pGEM-T plasmid and DNA fragments from 10 independent clones, and sequenced (PRIMM-Seq core Naples-Italy) to ensure that no mutation had occurred during the amplification. The gene PSHAa 1385 was then excised from the plasmid pGEM-T using *Bam*HI and *XhoI* restriction enzymes, and was separated on a 1% agarose gel and purified using a DNA gel extraction kit purchased from Stratagene. The fragment obtained was ligated into a pET28a expression vector digested with the same enzymes so that a six-histidine stretch was fused at the N-terminus of the recombinant module.

**Protein Expression.** N-terminus His6-S-tagged proteins from pET28a constructs were overexpressed following transformation in *E. coli* BL21(DE3). Cells were recovered and lysed by sonication (Soniprep; Sanyo) after growth at 37 °C on Luria−Bertani medium supplemented with kanamycin. Induction was carried out by adding 0.1 mM isopropyl-$\beta$-D-thiogalactopyranoside (IPTG) to a culture at an optical density of 0.5 measured at 600 nm, and then incubating the culture at 37 °C for 3 h. Protein constructs were purified by nickel affinity chromatography as described by the manufacturer (Novagen). Thrombin cutting on column was used to obtain the protein without the His stretch at its N-terminal. The purified protein was analyzed by SDS-PAGE and by Western Blotting with antibodies anti-His.

**Protein Determination and Enzyme Assay.** Protein concentration was determined using the BioRad protein staining assay and BSA as standard. The esterase activity was determined at temperatures ranging from 5 to 50 °C by using *p*-nitrophenyl-acetate (*p*NPAc) as substrate. The assay mixture (1 mL final volume), containing 5 mM *p*NPAc in 20 mM sodium phosphate buffer pH 7.4, and the assay started by adding the enzyme sample to the mixture. The release of *p*-nitrophenol was continuously monitored at 405 nm by a Cary UV−vis spectrophotometer equipped with a Dual Cell Peltier temperature controller (Varian). One enzyme unit was defined as the amount of enzyme releasing 1 $\mu$mol of *p*-nitrophenol per minute under the described conditions. Assay using α- and $\beta$-naphthyl acetate were analyzed following the release of α- or $\beta$-naphtol, monitored at 560 nm.[7] The enzyme assays, performed several time (at least five times) displayed always the same result indicating the high precision of the calculated PhEST activity.

**Molecular Dynamics Simulations and Analysis of the Results.** The structure of monomeric PhEST was modeled with a comparative modeling strategy, using as template the structure of *Saccharomyces cerevisiae* S-formylglutathione hydrolase,[11] available in PDB database[12] (PDB code: 1PV1), as previously described.[10] Molecular dynamics (MD) were carried out using the program *GROMACS* v 3.3.1[13,14] running in parallel (MPI) on a cluster with 40 × 86_64 Opteron processors. The GROMOS96 force field[15] was used throughout the simulations. The protein was included in a triclinic box with a distance of 0.75 nm per side from the protein, filled with 12 034 water molecules (SPC model)[16] and 15 $Na^+$ ions to neutralize the net negative charge of the whole system. Periodic boundary conditions were used to exclude surface effects. A preliminary energy minimization step with the Steepest Descent method with a tolerance of 1000 kJ/mol/nm was applied to the system. All bonds were constrained using LINCS.[17] Then, a short MD

simulation (20 ps) with position restraints was applied to soak the solvent into the macromolecule. The system was coupled to a temperature bath at 300 K and to a pressure of 1 atm using Berendsen's method.[18] Long-range electrostatics were handled using the PME method.[19] Cutoff was set at 0.9 nm for Coulomb interactions and at 1.4 nm for van der Waals interactions. Finally, three 10-ns-long simulations at 277, 293, and 318 K, respectively, were performed with a time step of 2 fs and without any position restraints.

Several analyses were conducted using programs built within the *GROMACS* package, and results were visualized and elaborated with the aid of the freely available program *Grace* (http://plasma-gate.weizmann.ac.il/Grace). The energy components were extracted from the energy files generated by the program, and analyzed to verify the stabilization of the system. For each simulation, an "average" structure representative of the trajectory was calculated, not including hydrogen atoms. Each "average" structure was saved in .pdb format, and was subsequently minimized with the Steepest Descent method as described above. Visualization and analysis of models was carried out using InsightII facilities. The accessibility of the residues to the solvent has been evaluated using the program *NACCESS*.[20]

**Phosphorescence Measurements.** Prior to phosphorescence measurements, PhEST was dialyzed against 2 mM Tris, pH = 8.0. In all samples, the final protein concentration was maintained between 8 and 10 $\mu$M. For low-temperature studies, the samples contained 60% (V/V) glycerol. For phosphorescence measurements in fluid solutions, particularly at ambient temperature, it is paramount to rid the solution of all $O_2$ traces. Protein samples were placed in oppositely constructed, 5 × 5 mm$^2$, quartz cuvettes deoxygenated by repeated cycles of mild evacuation followed by inlet of pure nitrogen as previously described.[21]

Phosphorescence spectra and phosphorescence decays were all measured with pulsed excitation ($\lambda_{ex}$ = 290 nm) on a homemade apparatus[22] modified to implement spectral measurements by means of CCD camera. Pulsed excitation was provided by a frequency-doubled Nd/Yag-pumped dye laser (Quanta Systems, Milano, Italy) with pulse duration of 5 ns and a typical energy per pulse of 0.5−1 mJ. For spectra measurements, the emission was collected at 90° from the excitation and dispersed by a 0.3 m focal length triplet grating imaging spectrograph (SpectraPro-2300i, Acton Research Corporation, Acton, MA) with a band-pass of 0.5 nm for high-resolution spectra in glasses and a band-pass of 2.0 nm for spectra in buffer at ambient temperature. The emission was monitored by a back-illuminated 1340 × 400 pixels CCD camera (Princeton Instruments Spec-10:400B (XTE), Roper Scientific Inc., Trenton, NJ) cooled to −60 °C. In low-temperature glasses, the phosphorescence spectrum was recorded after a 2 s delay from the exciting pulse in order to get rid of most of the short-lived emission from solvent impurities. This was achieved by opening a mechanical shutter, controlling the emission to the spectrograph, after a delay of 2 s. In fluid solutions, where the lifetime of tryptophan phosphorescence is much shorter than the 6 s of glassy media, spectra were recorded by integrating multiple excitation pulses at a repetition frequency up to 10 Hz. To block overlapping prompt fluorescence and short-lived background from reaching the detector, laser excitation was synchronized to a fast mechanical chopper opening the emission slit 50 $\mu$s after the laser pulse. In general, less than 20 pulses were sufficient to obtain satisfactory *S*/*N* ratios.

Phosphorescence decays were monitored by collecting the emission at 90° from vertical excitation through a filter combination with a transmission window of 405−445 nm (WG405, Lot-Oriel, Milano Italy, plus interference filter DT-Blau, Balzer, Milano, Italy). The photomultiplier (EMI 9235QA, Middlesex, UK) was protected against fatigue from the strong excitation/fluorescence pulse by either a gating circuit or a mechanical chopper synchronized to the laser trigger, which closed the emission slit during the excitation pulse. The time resolution of the latter option depends on the chopper speed and for the experiments reported here was maintained constant to 50 $\mu$s, the same as for spectral acquisitions. The photocurrent was amplified by a current-to-voltage converter (SR570, Stanford Research Systems, Stanford, CA) and digitized by a 16 bits high-speed (1.25 MHz) multifunction data acquisition board (NI 6250 PCI, National Instrument Italy, Milano, Italy) supported by *LABVIEW* software capable of averaging multiple sweeps. Typically, less than 20 sweeps were sufficient for a good signal-to-noise ratio even for the shortest decays. Prompt fluorescence was simultaneously collected through a 310−375 band-pass filter combination (WG305 nm plus Schott UG11) and detected by a UV-enhanced photodiode (OSD100−7, Centronics, Newbury Park, CA). The prompt fluorescence intensity was used to account for possible variations in the laser output between measurements as well as to obtain fluorescence-normalized phosphorescence intensities. All phosphorescence decays were analyzed in terms of discrete exponential components by a nonlinear least-squares fitting algorithm (DAS6, Fluorescence decay analysis software, Horiba Jobin Yvon, Milano, Italy). Each spectral and lifetime determination was repeated at least three times.

**$O_2$ and Acrylamide Quenching Experiments.** $O_2$ and acrylamide quenching experiments were carried as described before.[23,24] Briefly, the phosphorescence decay was measured at various quencher concentrations and the bimolecular quenching rate constant ($k_q$) was obtained from the slope of linear lifetime Stern−Volmer plots according to the equation

$$1/\tau = (1/\tau_0)+k_q[Q]$$

where $\tau_0$ and $\tau$ are the phosphorescence lifetime in the absence and in the presence of a given quencher concentration, [Q]. For $O_2$, the highest concentration employed was that of an aqueous solution in equilibrium with the atmosphere, as derived from the solubility of $O_2$ at various temperatures (280 $\mu$M at 20 °C). Smaller $O_2$ concentrations were determined from the lifetime of alkaline phosphatase, whose $k_q(O_2)$ is known over a wide temperature range, added to each protein sample under examination as described before.[23,24]

## Results and Discussion

Four Trp residues (W14, W50, W181, and W197) are present in PhEST. Their position and environment in the predicted structure are shown in Figure 1. W14 is at the beginning of the second strand forming the central $\beta$-sheet of each monomer, and it is largely exposed to the solvent (accessibility 46% and 46.8%, respectively, in subunits A and B). W50 is in the core of the molecule, in the central part of the $\beta$-sheet, at about 11 Å from the active site, and it is fully shielded from the solvent (accessibility 0% in both subunits). W181 is on an α-helix, approximately 10 Å from the active site, and is effectively shielded from the solvent (accessibility 7% in both subunits). Finally, W197 is on an external loop, partially exposed to the

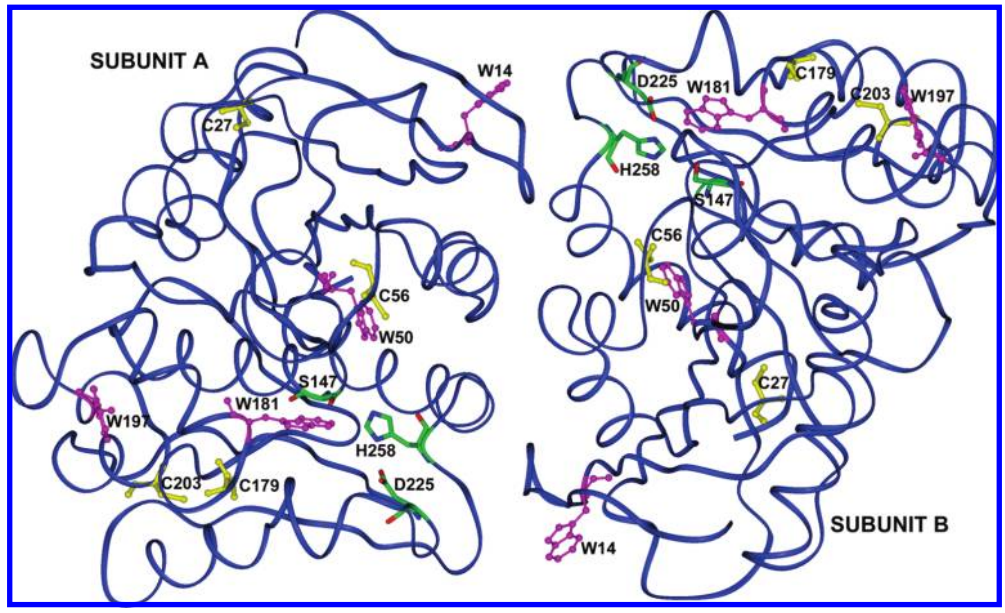


**Figure 1.** Model of dimeric PhEST with Trp residues (in magenta) and Cys residues (in yellow) represented in ball and stick mode. The residues of the active sites are color-coded and in stick mode.

**TABLE 1: Distances between Trp-Trp, Cys-Cys, and Trp-Cys in the Model and in the Average Structures at Different Temperatures**

| | distance (Å) in model | | distance (Å) at 277 K | | distance (Å) at 293 K | | distance (Å) at 318 K | |
|---|---|---|---|---|---|---|---|---|
| residues | subunit A | subunit B | subunit A | subunit B | subunit A | subunit B | subunit A | subunit B |
| W14−W50 | 22.16 | 22.16 | 22.29 | 21.55 | 20.74 | 22.34 | 21.83 | 21.12 |
| W14−W181 | 36.91 | 36.91 | 36.32 | 36.38 | 34.08 | 36.65 | 34.81 | 34.71 |
| W14−W197 | 45.38 | 45.37 | 43.05 | 46.20 | 44.30 | 45.39 | 42.20 | 44.22 |
| W50−W181 | 16.24 | 16.23 | 16.37 | 17.13 | 17.30 | 14.85 | 16.58 | 16.20 |
| W50−W197 | 25.81 | 25.80 | 25.20 | 27.48 | 26.94 | 24.88 | 23.80 | 27.19 |
| W181−W197 | 16.39 | 16.39 | 17.88 | 17.00 | 16.42 | 15.62 | 14.83 | 16.99 |
| C27−C56 | 19.82 | 19.56 | 20.79 | 18.65 | 19.34 | 19.58 | 18.25 | 19.89 |
| C27−C179 | 29.42 | 29.13 | 31.99 | 23.38 | 28.90 | 27.66 | 26.50 | 26.31 |
| C27−C203 | 31.92 | 31.49 | 35.22 | 29.07 | 31.45 | 30.06 | 30.72 | 30.75 |
| C56−C179 | 18.55 | 18.58 | 18.25 | 14.79 | 19.37 | 17.39 | 18.81 | 19.00 |
| C56−C203 | 22.37 | 22.37 | 23.58 | 22.18 | 21.96 | 20.38 | 26.74 | 24.11 |
| C179−C203 | 8.28 | 8.05 | 9.52 | 10.84 | 8.66 | 9.19 | 12.09 | 8.45 |
| C27−W14 | 30.57 | 30.52 | 26.63 | 28.23 | 27.88 | 30.77 | 28.32 | 29.10 |
| C27−W50 | 23.20 | 23.58 | 24.93 | 20.30 | 23.00 | 20.44 | 21.53 | 23.41 |
| C27−W181 | 23.91 | 23.64 | 26.18 | 20.95 | 20.23 | 22.13 | 17.52 | 21.34 |
| C27−W197 | 24.92 | 24.63 | 28.68 | 23.66 | 24.54 | 23.95 | 22.49 | 22.97 |
| C56−W14 | 25.71 | 25.70 | 25.62 | 25.73 | 23.43 | 27.40 | 24.57 | 24.42 |
| C56−W50 | 8.46 | 8.48 | 9.57 | 9.40 | 8.81 | 7.09 | 8.07 | 10.18 |
| C56−W181 | 11.58 | 11.61 | 11.34 | 11.25 | 11.20 | 9.61 | 11.49 | 11.53 |
| C56−W197 | 24.29 | 24.30 | 24.81 | 25.79 | 24.98 | 22.76 | 23.79 | 26.29 |
| C179−W14 | 41.62 | 41.64 | 41.20 | 38.94 | 41.80 | 42.61 | 40.74 | 40.09 |
| C179−W50 | 19.58 | 19.59 | 19.58 | 18.34 | 22.02 | 20.35 | 19.78 | 19.87 |
| C179−W181 | 9.11 | 9.07 | 8.46 | 5.09 | 10.77 | 9.10 | 11.52 | 8.65 |
| C179−W197 | 13.07 | 13.12 | 14.10 | 14.14 | 13.43 | 11.15 | 11.06 | 12.87 |
| C203−W14 | 41.44 | 41.60 | 42.03 | 42.30 | 41.53 | 40.86 | 44.09 | 44.55 |
| C203−W50 | 20.15 | 20.27 | 21.05 | 21.10 | 21.05 | 20.11 | 24.45 | 21.23 |
| C203−W181 | 16.09 | 15.88 | 16.73 | 15.66 | 16.73 | 15.60 | 21.29 | 16.07 |
| C203−W197 | 14.61 | 14.32 | 12.58 | 14.85 | 14.69 | 13.98 | 10.35 | 15.18 |

solvent (accessibility 29.5% in both subunits). The relative distances among these chromophores are reported in Table 1.

The analysis of the rms fluctuations of the residues at different temperatures, obtained from the molecular dynamics trajectories, allows the identification of the residues with higher conformational variability. These data indicate that the environments of W14 and of W50 are characterized by restricted conformational freedom. On the other hand, enhanced fluctuations of residues in the segments 93−99 and 192−195, even at the lowest simulated temperature (277 K), render the environments of W181 and W197 quite mobile (Figure 2). These two fragments correspond to flexible loops joining segments of secondary structure in the protein. W197 itself shows a marked conformational fluctuation.

The surroundings of each Trp residue were analyzed for the presence of quenching side chains (Cys, His, Tyr, and Phe) within interaction distance of the indole ring. Potential quenchers within a radius of 10 Å, in the static model and in the three average structures from the MD simulations, are reported in Table 2. While for each residue there are a number of potential quenchers, we anticipate that the proximity of W50 and of W181 to Cys residues is bound to dominate the phosphorescence

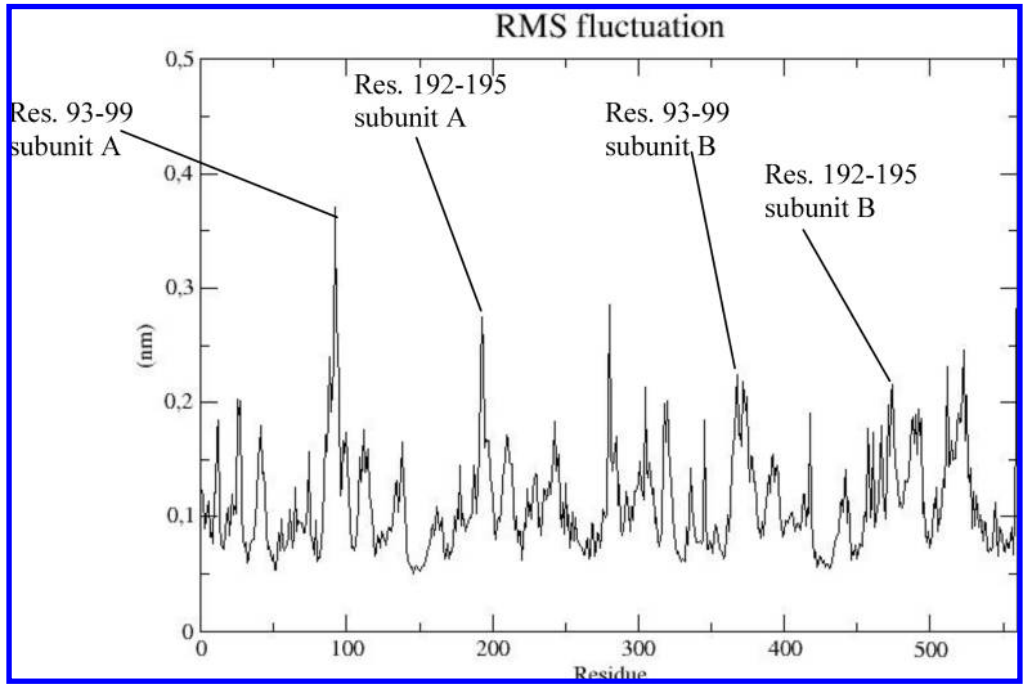


**Figure 2.** RMSF of PhEST at 277 K. The residues labeled are those with higher fluctuations in the spatial environment of W181 (res. 93−99) and W197 (res. 192−195).

**TABLE 2: Potential Quenchers in the Environment of Trp Residues**[a]

| residue | model | 277 K | 293 K | 318 K |
|---|---|---|---|---|
| Trp 14 | Y256 | H15, Y256 | H15, Y256 | H15, Y256 |
| Trp 50 | H146, H270, Y105, Y260, C56 | H146, H270, H274, Y105, Y260, C56 | H146, H270, H274, Y260, C56 | H146, H270, Y260, C56 |
| Trp 181 | H258, Y96, C179 | H146, H258, Y96, C179 | H258, Y96 | Y96 |
| Trp 197 | Y200 | Y200 | Y200 | H151, Y96 |

[a] Residues at less than 10 Å of distance are reported.

lifetime and quantum yield of these Trp residues over a wide temperature range.

**Phosphorescence Spectrum at 77 K.** In low temperature glasses, the phosphorescence spectrum of Trp generally displays a pronounced vibronic structure with a relatively well-resolved 0,0 vibrational band. While the wavelength of the 0,0 band ($\lambda_{0,0}$) is related to the polarity of the indole environment, its bandwidth (BW = the width at half height) reports on the structural homogeneity of the site.[25]

The phosphorescence spectrum of PhEST was monitored in glycerol/buffer at 77 to 260 K. The phosphorescence spectrum of PhEST in glycerol/buffer (60/40, v/v) at 77 K is shown in Figure 3. The spectrum is clearly the superposition of two or more distinct spectral components: one is characterized by a narrow 0,0 band peaked at 411.75 nm and the remainder by a blue-shifted broad shoulder centered at 407.5 nm. The former emission is typical of Trp residues embedded in nonpolar protein cores,[25] with the narrow BW implying a well-ordered homogeneous environment. A narrow BW also suggests that only a single residue contributes to this phosphorescence emission, as the likelihood that residues in distinct locations of the globular fold make exactly the same interaction with the protein surrounding is rather remote. The broad blue spectral component, on the other hand, is characteristic of Trp residues in polar sites or exposed to the aqueous solvent ($\lambda_{0,0}$ = 407.5 nm for free Trp in this solvent). The low resolution of the blue 0,0 band may be due to the sum of imperfectly overlapping spectra from different Trp residues and/or to intrinsically broad contributions from residues exposed to the solvent or located in conformationally disordered regions. On the basis of the relative intensity of the blue and red bands, we deduce that the Trp residues contributing to the former are poor emitters, presumably due to a below average fluorescence quantum yield.

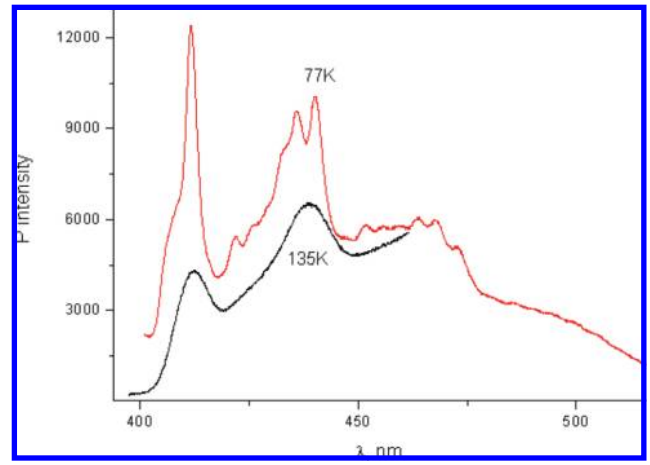


**Figure 3.** Trp phosphorescence spectrum of PhEST in glycerol/buffer (60/40, v/v) at selected temperatures. The protein concentration was 9 $\mu$M; $\lambda_{ex}$ = 290 nm. Spectral intensities are offset for clarity.

**Thermal Profile of P Spectrum.** Warming the glass into a fluid solution confers flexibility to the protein structure, and following its relaxation about the excited chromophore the phosphorescence spectrum generally undergoes sizable red-shift and broadening. Concomitant to spectral changes, there are more or less drastic reductions in phosphorescence yields caused by the general shortening of the phosphorescence lifetime in fluid

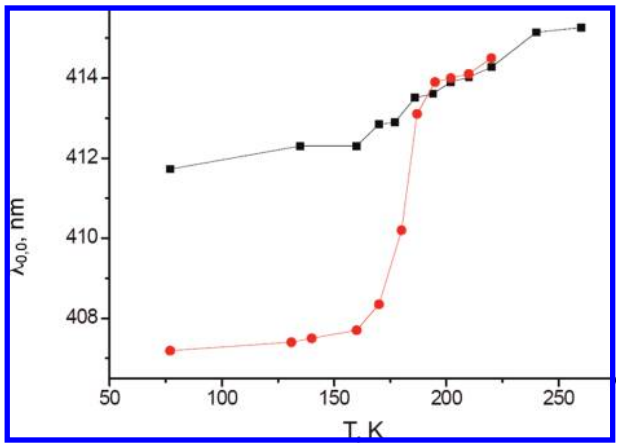


**Figure 4.** Peak wavelength of the 0,0 band ($\lambda_{0,0}$) of the phosphorescence spectrum of PhEST (■) and of free Trp (•) at increasing temperature in a 60/40 glycerol/buffer solution. Other conditions are as described in Figure 3.

media plus the potential onset of thermally activated intramolecular quenching reactions.

The phosphorescence spectrum of PhEST was monitored in glycerol/buffer from 77 to 260 K. The thermal profile illustrates the relaxation (red-shift)/quenching of individual spectral components upon increasing the temperature/decreasing solvent viscosity. Figure 3 shows that the main change of the phosphorescence spectrum of PhEST occurs on raising the temperature from 77 to 135 K: the spectrum became broad and red-shifted with a total loss of the fine vibrational structure that distinguishes the two spectral components.

This finding is unusual, because even if below the $T_g$ global motions still exist on a very long time scale (the glass transition temperature ($T_g$) of the solvent is about 190 K), we did not expect spectral changes at these low temperatures where the glass is still quite rigid and protein and solvent motions are blocked. Raising temperature from 77 to 135 K apparently brings a significant quenching/red-shift of both the blue (407 nm shoulder) and the red (411.75 nm) spectral components. From the spectral shift, it would appear that the environment of the putative Trp residues possesses a flexibility larger than that of the solvent in rigid glasses. Intramolecular quenching reactions at these low temperatures are effective only in the presence of nearby Cys, as quenching by His and Tyr generally requires mobility and becomes effective only in fluid solutions.[21] Above 135 K, the spectrum broadens further and red-shifts in a gradual, continuous manner (Figure 4) without any abrupt change in correspondence of $T_g$, when the solvent becomes fluid. A limited red-shift at $T_g$ is consistent with a phosphorescence emission originating largely from buried Trp residues, while the low spectral resolution presumably reflects conformational disorder due to structural flexibility.

**Phosphorescence Lifetime in Buffer at Selected pH and Temperature Values.** The intrinsic phosphorescence lifetime ($\tau_0$) in room-temperature aqueous solution is generally a direct monitor of protein flexibility in the region surrounding the chromophore.[21,26] In proteins, $\tau$ decreases from the limiting value of 5−6 s in rigid glasses up to tens of microseconds in aqueous room-temperature solutions, the reduction of $\tau$ reflecting the onset of structural fluctuations enhancing both the radiationless deactivation of the excited triplet state as well as the diffusion of quenching solutes, such as impurities in the solvent. Although internal residues within compact folds are expected to exhibit second-long lifetimes, the onset of intramolecular quenching reactions with nearby Cys, His, and Tyr side chains may reduce their lifetimes to the microsecond−millisecond domain.[21]

The phosphorescence decay of PhEST in Tris buffer, pH 8 and 20 °C, is heterogeneous and unusually short for buried Trp residues. When fitted to a biexponential function, it yields lifetimes $\tau_1 = 0.22$ ms (41%) and $\tau_2 = 0.95$ ms (59%). While millisecond lifetimes are typical of solvent-exposed residues,[22] they are unduly short for buried chromophores and clearly indicate that in such cases $\tau$ is dominated by intramolecular quenching processes. In model peptides, quenching reactions are characterized by relatively low activation energies, $E_a \approx 2-6$ kcal/mol,[21] compared to 8−30 kcal/mol typical for structural fluctuations,[27] and by a dependence on pH that is specific of the quenching side chain.[21] To investigate $E_a$, we have measured the decay in the −5 to 30 °C temperature range. The Arrhenius plot of the average decay rate [$1/\tau_{av} = 1/(\alpha_1\tau_1 + \alpha_2\tau_2)$] yielded $E_a = 3.0$ kcal/mol, a value more in line with a quenching reaction rather than with protein dynamics.

The pH dependence of His and Tyr quenching foresees a sharp, 2−3 order of magnitude, increase of the rate as the pH is lowered below the respective p$K_a$, whereas for Cys, the rate is relatively constant with pH.[21] Decay measurements showed that from pH 7.0 to pH 11 the phosphorescence lifetime was practically unaffected by pH, whereas $\tau_{av}$ decreased by only two folds on lowering the pH from 7 to 5. This result rules out the possibility that Tyr and His be important quenchers. The remaining possibilities are as follows: (1) quenching by a nearby Cys and/or (2) by triplet−triplet energy transfer from internal Trp to a nearby Trp that is itself quenched by Cys.

**Acrylamide and $O_2$ Quenching of PhEST Phosphorescence.** Molecular oxygen and acrylamide are strong quenchers (Q) of Trp phosphorescence. Their migration through the protein fold to the site of Trp causes a shortening of the lifetime according to the expression

$$1/\tau = 1/\tau_0 + k_q[Q]$$

where $k_q$ is the bimolecular quenching rate constant and [Q] is the oxygen or acrylamide concentration in solution. $k_q$ is essentially determined by the diffusion coefficient of Q through the protein matrix, and the ratio $k_q$(protein)/$k_q$(Trp), $k_q$(Trp) is the rate constant for free Trp in aqueous solution, represents the factor by which Q migration in the protein is slowed down relative to its diffusion in water. Hence, the $k_q$ ratio represents a sensitive monitor of the frequency of structural fluctuations of sufficiently large amplitude to permit the internal migration of the quencher. Since acrylamide is a much larger molecule than $O_2$, its migration will be considerably slower and will report selectively on fluctuations of considerably larger amplitude.

For acrylamide quenching of free Trp, $k_q = 1.2 \times 10^9$ $M^{-1}$ $s^{-1}$ [3] and, consequently, millimolar concentrations of acrylamide are sufficient to effectively quench external and superficial Trp residues. At 20 °C, measurements of the phosphorescence lifetime of PhEST as a function of acrylamide concentration showed that the phosphorescence decay is affected only in the low concentration range, 40 mM acrylamide eliminating completely the very short and the longest, 0.9 ms, lifetime components of the decay, making the remaining emission rather homogeneous with $\tau = 0.63$ ms (Figure 5). Further increases in acrylamide concentration, up to 0.5 M, do not affect $\tau$. In fact, the only change of the phosphorescence emission is a moderate reduction in phosphorescence intensity that is accounted for by the quencher inner filter. According to the accessibility of acrylamide, we can distinguish at least two

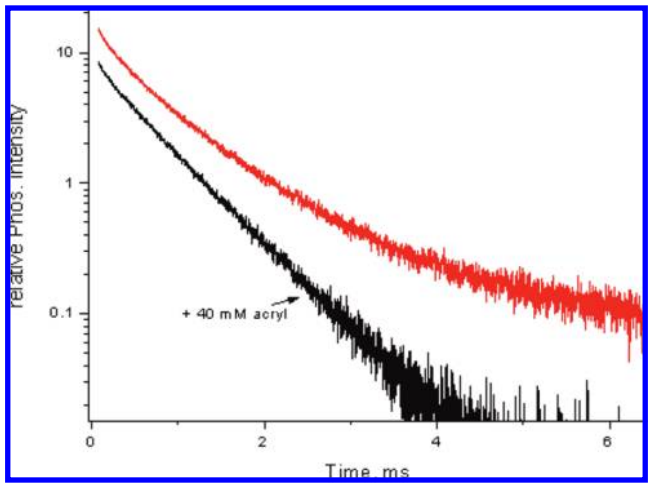


**Figure 5.** Trp phosphorescence decay of PhEST in buffer (2 mM Tris, pH 8) and after the addition of 40 mM acrylamide at 20 °C. The protein concentration was 10 $\mu$M; $\lambda_{ex}$ = 290 nm.

classes of Trp residues that contribute to the room-temperature phosphorescence emission of the enzyme. In particular, the readily quenched fraction of the emission refers to superficial and partially solvent exposed residues, whereas the unquenched fraction refers to highly shielded chromophores. For the latter, one may estimate an upper bound for $k_q$ of $5 \times 10^2$ $M^{-1}$ $s^{-1}$. This is a relatively small value and in other proteins is characteristic of deep compact cores involving large $\beta$-sheet structures.[23] Confirmation of the rigidity of this internal site was provided by the $O_2$ quenching rate constant. The rate constant for the $O_2$ quenching, derived by a two-point Stern−Volmer plot (data not shown) was $7.1 \times 10^6$ $M^{-1}$ $s^{-1}$, which is a thousand-fold smaller than $k_q$(Trp) and similar to that obtained for the $\beta$-barrel core of azurin.[24]

**Consistency between the Protein Model Structure and Phosphorescence Properties of PhEST.** According to the model structure, W14 is exposed to the solvent near the dimer subunit interface. Its phosphorescence spectrum in glasses is expected to be broad, with $\lambda_{0,0}$ = 407−408 nm, and to relax to the red around $T_g$. Since no quenching side chain is in its proximity, its lifetime in buffer at room temperature should be approximately 1 ms or smaller.[22,26] Because of its direct accessibility to the solvent, it is expected to be readily quenched by millimolar acrylamide solutions.

W181 and W197 are both located in the same flexible loop region of the polypeptide, within fluorescence energy transfer distance (1.6 nm) of each other. Both are in partly solvent exposed flexible sites, generally characterized by a relatively broad phosphorescence spectrum. Their emission is expected to be considerably quenched in fluid media due to the proximity of quenching side chains, namely, Y96 (at 0.34 nm) and C179 (at 0.84 nm) in the case of W181 and by the ring stacking configuration of F186 in the case of W197 (Table 2). As a result, little room-temperature phosphorescence is expected from this couple of residues (sub-microsecond lifetime) and any emission would be readily accessible to external quenching.

Last, W50 is deeply buried within the $\beta$-sheet core of the subunit, surrounded by mostly hydrophobic side chains (L48, I78, A67, F170, F61, H146, and Y260). It is a mostly rigid, well-ordered hydrophobic site expected to yield a sharply resolved spectrum at 77 K with $\lambda_{0,0}$ = 411−412 nm. This residue is highly inaccessible to external quenchers like acrylamide, and even for small molecules like $O_2$, internal migration is expected to be drastically hindered. The emission of W50, however, is dominated by the interaction with C56, which is only 0.66 nm away (average closest distance between the sulfur atom and an atom of the indole ring). At 77 K, Cys quenching of Trp phosphorescence is negligible,[28,29] and therefore, the emission of W50 is expected to be intense. However, because of the sharp temperature dependence of the Cys interaction[26,28] quenching is expected to become important when the temperature is raised to 135 K. As a consequence, the well-resolved and intense emission observed at 77 K is expected to become considerably quenched at 135 K, even if the glass is still rigid at this temperature (no other internal quencher has this property). At room temperature, the interaction is even stronger and is expected to conduct to a sub-millisecond lifetime. Using the distance dependence of the indole−Cys interaction at 20 °C, derived with model compounds assuming no orientation dependence of the interaction[30] [$k(r) = 4 \times 10^9 \exp[-40(r - r_0)]$ $s^{-1}$, $r_0$ = 0.3 nm] the above separation from C56 predicts ($k(0.66) = 2200$ $s^{-1}$) a lifetime for W50 of about 0.5 ms ($1/\tau \approx k(r)$). Further, because the decay rate is dominated by intramolecular quenching rather than by structural flexibility, the lifetime of W50 is expected to be weakly dependent on temperature ($E_a \approx 3$ kcal/mol). To confirm these spectroscopic results, we decided to generate PhEST mutant variants. Unfortunately, the recombinant mutant PhEST proteins were mainly obtained as inclusion body. Even if a small amount of mutant forms of Phest was obtained, we noticed that the mutant forms were very unstable as observed by their aggregation and precipitation during the phosphorescence measurements.

In conclusion, if we assign the sharp red band in the phosphorescence spectrum of PhEST to W50 and the composite broad blue component to W14, W181, and W197 we find that all the phosphorescence properties of the protein listed above are fully consistent with the protein model structure.

**Acknowledgment.** This project was realized in the frame of the CNR Commessa "Diagnostica Avanzata ed Alimentazione", and was also partially supported by CNR-Bioinformatics project. The authors are indebted with Prof. Mariorosario Masullo, and Prof. Paolo Arcari from the Dipartimento di Biochimica e Biotecnologie Mediche, Università di Napoli Federico II, via S. Pansini 5, 80131 Napoli, Italy for providing the biomass of *Pseudoalteromonas haloplanktis,* and with Dr. Umberto Amato for hosting MD simulations on the cluster "Lilligrid" located at the IAC−CNR, Naples.

## References and Notes

(1) Morita, R. Y. *Bacteriol. Rev.* **1975**, *39*, 144.
(2) Siddiqui, K. S.; Cavicchioli, R. *Annu. Rev. Biochem.* **2006**, *75*, 403.
(3) Fields, P. A.; Somero, G. N. *Proc. Natl. Acad. Sci. U.S.A.* **1998**, *95*, 11476.
(4) D'Amico, S.; Gerday, C.; Feller, G. *Gene* **2000**, *253*, 95.
(5) Cavicchioli, R.; Siddiqui, K. S.; Andrews, D.; Sowers, K. R. *Curr. Opin. Biotechnol.* **2002**, *13*, 253.
(6) Georlette, D.; Blaise, V.; Collins, T.; D'Amico, S.; Gratia, E.; Hoyoux, A.; Marx, J.-C.; Sonan, G.; Feller, G.; Gerday, C. *FEMS Microbiol. Rev.* **2004**, *28*, 25.
(7) Aurilia, V.; Parracino, A.; Saviano, M.; D'Auria, S. *Gene* **2007**, *397*, 51.
(8) Médigue, C.; Krin, E.; Pascal, G.; Barbe, V.; Bernsel, A.; Bertin, P. N.; Cheung, F.; Cruveiller, S.; D'Amico, S.; Duilio, A.; Fang, G.; Feller, G.; Ho, C.; Mangenot, S.; Marino, G.; Nilsson, J.; Parrilli, E.; Rocha, E. P.; Rouy, Z.; Sekowska, A.; Tutino, M. L.; Vallenet, D.; von Heijne, G.; Danchin, A. *Genome Res.* **2005**, *15*, 1325.
(9) Aurilia, V; A.; Parracino, A; D'Auria, S *Gene* **2008**, *410*, 234.
(10) Aurilia, V.; Rioux-Dubé, J. F.; Marabotti, A.; Pézolet, M.; D'Auria, S. *J. Phys. Chem. B* **2009**, *113*, 7753.
(11) Legler, P. M.; Kumaran, D.; Swaminathan, S.; Studier, F. W.; Millard, C. B. *Biochemistry* **2008**, *47*, 9592.

(12) Berman, H.; Henrick, K.; Nakamura, H.; Markley, J. L. *Nucleic Acids Res.* **2007**, *35* (Database issue), D301.
(13) Lindahl, E.; Hess, B.; van der Spoel, D. *J. Mol. Model.* **2001**, *7*, 306.
(14) van der Spoel, D.; Lindahl, E.; Hess, B.; Groenhof, G.; Mark, A. E.; Berendsen, H. J. C. *J. Comput. Chem.* **2005**, *26*, 1701.
(15) van Gunsteren, W. F.; Billeter, S. R.; Eising, A. A.; Hunenberger, P. H.; Kruger, P.; Mark, A. E.; Scott, W. R. P.; Tironi, I. G. *Biomolecular Simulation: The GROMOS96 Manual and User Guide*; Vdf Hochschulverlag AG an der ETH Zurich: Zurich, Switzerland, 1996; p 1042.
(16) Berendsen, H. J. C.; Postma, J. P. M.; van Gunsteren, W. F.; Hermans, J. In *Intermolecular Forces*, Pullman, B., Ed.; Reidel D. Publishing Company: Dordrecht, The Netherlands, 1981; pp 331−342.
(17) Hess, B.; Bekker, H.; Berendsen, H. J. C.; Fraaije, J. G. E. M. *J. Comput. Chem.* **1997**, *18*, 1463.
(18) Berendsen, H. J. C.; Postma, J. P. M.; van Gunsteren, W. F.; Di Nola, A.; Haak, J. R. *J. Chem. Phys.* **1984**, *81*, 3684.
(19) Essmann, U.; Perera, L.; Berkowitz, M. L.; Darden, T.; Lee, H.; Pedersen, L. G. *J. Chem. Phys.* **1995**, *103*, 8577.
(20) Hubbard, S. J.; Campbell, S. F.; Thornton, J. M. *J. Mol. Biol.* **1991**, *220*, 507.
(21) Gonnelli, M.; Strambini, G. B. *Photochem. Photobiol.* **2005**, *81*, 614.
(22) Strambini, G. B.; Kerwin, B. A.; Mason, B. D.; Gonnelli, M. *Photochem. Photobiol.* **2004**, *80*, 462.
(23) Cioni, P.; Strambini, G. B. *J. Am. Chem. Soc.* **1998**, *120*, 11749.
(24) Strambini, G. B.; Cioni, P. *J. Am. Chem. Soc.* **1999**, *121*, 8337.
(25) Hershberger, M. V.; Maki, A. H.; Galley, W. C. *Biochemistry* **1980**, *19*, 2204.
(26) Strambini, G. B.; Gonnelli, M. *J. Am. Chem. Soc.* **1995**, *117*−7646.
(27) Cioni, P.; Strambini, G. B. *J. Mol. Biol.* **1999**, *291*, 955.
(28) Li, Z.; Bruce, A.; Galley, W. C *Biophys. J.* **1992**, *61*, 1364.
(29) Li, Z.; Lee, W. E.; Galley, W. C *Biophys. J.* **1989**, *56*, 361.
(30) Lapidus, L. J.; Eaton, W. A.; Hofrichter, J. *Phys. Rev. Lett.* **2001**, *87*, 258101.

JP9043286